IEEE Access
Multidisciplinary | Rapid Review | Open Access Journal

Received March 19, 2020, accepted April 1, 2020, date of publication April 13, 2020, date of current version May 4, 2020.

Digital Object Identifier 10.1109/ACCESS.2020.2987469

On the Disturbance Rejection of a Piezoelectric Driven Nanopositioning System

WEI WEI[1], PENGFEI XIA[2], WENCHAO XUE[3], (Member, IEEE), AND MIN ZUO[4]

[1]School of Computer and Information Engineering, Beijing Technology and Business University, Beijing 100048, China
[2]National Engineering Laboratory for Agri-product Quality Traceability, Beijing Technology and Business University, Beijing 100048, China
[3]Academy of Mathematics and Systems Science, Chinese Academy of Sciences, Beijing 100049, China
[4]Beijing Key Laboratory of Big Data Technology for Food Safety, Beijing Technology and Business University, Beijing 100048, China

Corresponding author: Min Zuo (zuomin@btbu.edu.cn)

This work was supported in part by the National Natural Science Foundation of China under Grant 61873005 and Grant 61403006, in part by the Key Program of Beijing Municipal Education Commission, China, under Grant KZ201810011012, and in part by the Support Project of High-level Teachers in Beijing Municipal Universities in the Period of 13th Five-year Plan, China, under Grant CIT&TCD201704044.

ABSTRACT Nanopositioning systems are very popular and playing an increasingly vital role in micro and nano-scale positioning industry due to their unique ability to achieve high-precision and high-speed operation. However, hysteresis, commonly existing in piezoelectric actuators, degrades the precision seriously. Uncertain dynamics and sensor noises also greatly affect the accuracy. To address those challenges, a variable bandwidth active disturbance rejection control (VBADRC) is proposed and realized on a nanopositioning stage. All undesired issues are estimated by a time-varying extended state observer (TESO), and cancelled out by a variable bandwidth controller. Convergence of the TESO, advantages of a TESO over a linear extended state observer (LESO), and the closed-loop stability of the VBADRC are proven theoretically. Improvements of the VBADRC versus the linear active disturbance rejection control (LADRC) are validated by simulations and experiments. Both numerical and experimental results demonstrate that the VBADRC is not only able to provide the same disturbance estimation ability as the LADRC, but also more powerful in noise attenuation and reference tracking.

INDEX TERMS Nanopositioning, active disturbance rejection control, time-varying extended state observer, variable bandwidth control, noise attenuation

I. INTRODUCTION

Nanopositioning is a key technology in modern precision and ultrahigh-precision manufacturing, such as atomic force microscope (AFM), biological micromanipulation, and precision mirror alignment [1]–[3]. For sub-nanometer resolution, fast response, large stiffness, and large blocking force, piezoelectric actuator (PZT) has been widely utilized as a crucial component in nanopositioning stages [4]. However, hysteresis, the dominant nonlinearity of a PZT, results in current displacement of a PZT not only depending on its current input signal but also depending on its past displacements [5]. In addition, for PZTs' rate dependence, the frequency of a PZT's input also affects its dynamics. Therefore, when the control signal changes, behaviors of PZTs also change distinctly. Furthermore, creep and lightly damped resonant dynamics introduced by a PZT will also decrease positioning performance. Those particular properties of a PZT make desired nanopositioning be a challenge.

To address it, numerous control algorithms have been proposed to improve the precision. Recently, state-of-art surveys are presented in [4], [6], [7]. Control structure can be classified into feed-forward control, feed-back control, feed-forward and feed-back control [4]. Basic ideas are hysteresis inversion model based feed-forward and (or) feed-back approaches [8]–[10], and hysteresis inversion model free approaches, respectively [11]–[13]. Hysteresis inversion model based approaches need accurate hysteresis model and inverse hysteresis model. It is time and cost consuming. In addition, most inversion-based methods only take effect in low-frequency cases [11]. Furthermore, inversion-based methods are not robust to external disturbances and the inaccurate inversions [11].

For overcoming limitations of inversion-based approaches, inversion free methods have been proposed. If hysteresis is viewed as a bounded disturbance, a nanopositioning

The associate editor coordinating the review of this manuscript and approving it for publication was Lei Wang.

system driven by a PZT can be treated as a system with bounded disturbance. Numerous disturbance rejection or disturbance attenuate approaches have been reported. Sliding mode control (SMC) is adopted to attenuate disturbances [12], [14], [15], and it presents good performance. However, the infinite gain problem and the chattering phenomenon involved in SMC [11] also limit its applications. Considering parametric uncertainties, model estimation errors and un-modeled dynamics, adaptive perturbation estimation has been proposed for the trajectory tracking in piezoelectric position [16]. Active disturbance rejection control (ADRC) has been exploited to estimate and suppress the uncertainties arising from hysteresis, creep, and other unknown disturbances [17]. However, those ways do not take sensor noises into consideration. The output is noisy, and noises do affect performance. In presence of noises, a solution to estimate disturbance effectively is more desired.

ADRC is a promising tool in dealing with disturbances and uncertainties due to its powerful ability in estimation and compensation. Above all, such ability is achieved before disturbances and uncertainties affect the system output. So far, there are a wide range of applications [18]–[21]. It is reasonable that ADRC may be a suitable tool for a nanopositioning stage to get desired positioning. Actually, for ADRC, the extended state observer (ESO) is critical to guarantee the closed-loop performance. Numerous modified ESOs [22]–[24] have been proposed to improve a classical ESO. A nonlinear ESO with time varying gain is designed to avoid the output of an ESO being large [22]. A special kind of nonlinear ESO is put forward to ensure desired estimation errors [23]. However, those results do not take consideration of sensor noises, which are inevitable in practical processes. To address noises, estimation errors can be minimized in stochastic sense by using dynamic gains for an ESO [24]. Nevertheless, it usually needs some statistic information of the measurement noises. On the other hand, some special structures, such as filters, are necessary. However, if filters are utilized, additional phase delays are inevitable. Absolutely, it is unexpected for real time control.

To this end, in this paper, a modified ADRC is presented. To enhance the performance in presence of noises, a time varying extended state observer (TESO) is utilized [25]. By comparison with those available ESOs, the TESO can recover the estimation performance in initial phase and achieving better noise filtering in steady phase. Additionally, based on the control errors, a variable bandwidth controller (VBC) is also designed. A TESO and a VBC constitute a variable bandwidth active disturbance rejection control (VBADRC). In order to verify the VBADRC, a linear ADRC (LADRC) has been presented for comparisons. Both numerical and experimental results have been given to confirm the proposed approach.

The major contribution of this paper is the development of a VBC and a VBADRC algorithm. Without introducing any filter or other special structures, the TESO can address sensor noises in its unique way, and no extra phase delay is introduced. In addition, based on control errors, the VBC guarantees tracking performance. Advantages of a TESO and a VBC ensure advantages of the VBADRC, and it is validated on a piezo-driven nanopositioning platform. Realtime control responses coincide with the theoretical results.

The paper is organized as follows. Section II presents the concerned problem. The LADRC is introduced and the VBADRC is developed in Section III. Numerical results and experimental results are given out in Section IV and Section V, respectively. Conclusions are summarized in Section VI.

II. PROBLEM STATEMENTS

A model describing dynamics of a nanopositioning stage can be written as [4], [12], [26]

$$M\ddot{x}(t) + B\dot{x}(t) + Kx(t) = Du(t) + H(t) + Q(t) \tag{1}$$

where t is the time variable. M, B, K and D are mass, damping coefficient, stiffness, and piezoelectric coefficient of a nanopositioning stage, respectively. Additionally, u is the control signal that drives the stage to track desired trajectories, x is the output displacement of the stage, H represents the hysteresis of a system, and $Q(t)$ denotes disturbances and uncertainties.

A cascaded model structure of a piezo-actuated nanopositioning stage can be depicted in Fig. 1 [26].

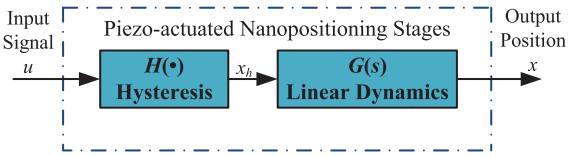

FIGURE 1. A cascade model of a piezoelectric driven nanopositioning system.

System dynamics can be rewritten as

$$\ddot{x}(t) + a_1\dot{x}(t) + a_0x(t) = q_0u(t) + d(t) \tag{2}$$

where $a_1 = \dfrac{B}{M}$, $a_0 = \dfrac{K}{M}$, $q_0 = \dfrac{D}{M}$, $d(t) = \dfrac{H(t) + Q(t)}{M}$.

In this paper, instead of identifying exact models of the hysteresis and other uncertainties, hysteresis and uncertainties are regarded to be a part of the generalized disturbance. By estimating and compensating them as a signal, from the view of active disturbance rejection control, desired trajectories can be tracked.

To simplify the representation, time variable t is omitted in following sections.

III. TIME VARYING ACTIVE DISTURBANCE REJECTION CONTROL

In this section, linear active disturbance rejection control (LADRC) is introduced first. Then, considering both disturbance rejection and sensor noises suppressing, a variable bandwidth active disturbance rejection control (VBADRC) is proposed.

A. LINEAR ACTIVE DISTURBANCE REJECTION CONTROL

Actually, system (2) can be rewritten as

$$\begin{cases} \dot{x}_1 = x_2 \\ \dot{x}_2 = f(x_1, x_2, u, d, t) + b_0 u \\ y = x_1 + n \end{cases} \tag{3}$$

if one let $x = x_1, \dot{x} = x_2, f(x_1, x_2, u, d, t) = -\frac{K}{M}x_1 - \frac{B}{M}x_2 + (\frac{D}{M} - b_0)u + \frac{H(t) + Q(t)}{M}$.

Here x_1, x_2 are system states, u is the control input, n is the sensor noise, y is the output, b_0 is the tunable coefficient of a control input, d is the disturbance, t is the time variable, and $f(x_1, x_2, u, d, t)$ represents the uncertain dynamics, it is also known as a generalized disturbance.

Control law of the LADRC for system (3) can be designed as [27]

$$u = \frac{k_{pl}(y_r - z_{l1}) - k_{dl}z_{l2} - z_{l3}}{b_0} \tag{4}$$

where k_{pl}, k_{dl} and b_0 are tunable parameters, y_r is the desired output, and z_{l1}, z_{l2}, z_{l3} are states of a LESO, which can be designed as [27]

$$\begin{cases} \dot{z}_{l1} = z_{l2} + \beta_1(y - z_{l1}) \\ \dot{z}_{l2} = z_{l3} + \beta_2(y - z_{l1}) + b_0 u \\ \dot{z}_{l3} = \beta_3(y - z_{l1}) \end{cases} \tag{5}$$

where β_1, β_2 and β_3 are tunable gains, y is the system output, and u is the control input. z_{l1}, z_{l2} and z_{l3} estimate x_1, x_2 and the generalized disturbance $f(x_1, x_2, u, d, t)$, respectively. Control block diagram of the 3rd order LADRC is given in Fig. 2.

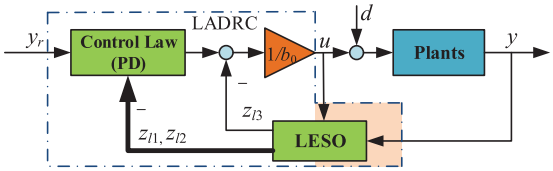

FIGURE 2. Structure of the 3rd order LADRC.

Substituting control law (4) into system (3), one has the closed-loop system

$$\begin{cases} \dot{x}_1 = x_2 \\ \dot{x}_2 = -k_{pl}(x_1 - y_r) - k_{dl}x_2 + k_{pl}\bar{e}_1 + k_{dl}\bar{e}_2 + \bar{e}_3 \end{cases}$$

where estimation errors $\bar{e}_1, \bar{e}_2, \bar{e}_3$ are defined as

$$\begin{cases} \bar{e}_1 = x_1 - z_{l1} \\ \bar{e}_2 = x_2 - z_{l2} \\ \bar{e}_3 = f - z_{l3} \end{cases}$$

Obviously, if parameters of the controller (4) and the LESO (5) are properly chosen, i.e. the controller works and the LESO converges, the closed-loop system is stable. Furthermore, for nonlinear system (3), better linearization can be obtained, if much smaller estimation errors $\bar{e}_1, \bar{e}_2$ and $\bar{e}_3$ can be guaranteed. In other words, by choosing proper parameters $k_{pl}, k_{dl}, \beta_i (i = 1, 2, 3)$, one can get desired system performance.

B. VARIABLE BANDWIDTH ACTIVE DISTURBANCE REJECTION CONTROL

Although LADRC is commonly used for its satisfied performance and practical design, measurement noises are not considered in its design. However, the noises definitely affect the tracking accuracy and control energies. Therefore, a TESO is designed to deal with both the generalized disturbance and the sensor noises. At the same time, a VBC is also proposed to guarantee the tracking performance. In other words, a VBADRC, which consists of a TESO and a VBC, is able to guarantee the tracking accuracy and reduce the control energies in presence of sensor noises.

1) VARIABLE BANDWIDTH ACTIVE DISTURBANCE REJECTION CONTROL DESIGN

From Section III. A, one can see clearly that the key point of LADRC is to convert the nonlinear uncertain system into an approximately linear system by a LESO. If a LESO is capable of estimating system states and the generalized disturbance faster and more accurately, the disturbance and uncertainties can be cancelled out timely and effectively. Thus, the closed-loop system performance can be greatly improved.

Generally, gains of a LESO are designed to be functions of a bandwidth parameter [27]. Larger bandwidth generates faster convergence of the estimation error, but it also means that the output is corrupted by the sensor noise worse.

Actually, for an ESO, generalized disturbance estimation is the main purpose in the initial state, and noise filtering is the key task in the steady state [25]. Therefore, an ESO with time-varying gains, which is able to guarantee both estimation in the transient process and filtration in the steady state, can be designed as

$$\begin{cases} \dot{z}_1 = z_2 + \beta_1(y - z_1) \\ \dot{z}_2 = z_3 + \beta_2\rho(t)(y - z_1) + b_0 u \\ \dot{z}_3 = \beta_3\rho(t)(y - z_1) \end{cases} \tag{6}$$

where z_1, z_2 and z_3 are states of the TESO, which estimate x_1, x_2 and the generalized disturbance of system (3), y is the output of (3), $\beta_1, \beta_2, \beta_3$ are tunable gains of the TESO, u is the control input, and $\rho(t)$ is a smoothly decreasing function.

In this paper, $\rho(t)$ is chosen to be

$$\rho(t) = (\rho_0 - \rho_\infty)e^{-lt} + \rho_\infty \tag{7}$$

where l is the decreasing rate, and

$$\begin{cases} \rho_0 \triangleq \rho(0) > 0 \\ \rho_\infty \triangleq \lim\limits_{t\to\infty} \rho(t) > 0, \forall t \geq 0 \\ \dot{\rho}(t) \leq 0 \end{cases} \tag{8}$$

Obviously, gains of z_2 and z_3 in a TESO are smoothly decreasing with respect to time variable t. ρ_∞ determines

final gains of z_2 and z_3. It can be seen later that the noise attenuation level is determined by ρ_∞.

For a TESO, a controller, which is able to adapt to control errors, is necessary to guarantee the closed-loop tracking performance. In this paper, a variable bandwidth control law is designed, and it can be depicted as,

$$u = \frac{k_p(y_r - z_1) - k_d z_2 - z_3}{b_0} \tag{9}$$

Here, k_p and k_d are time-varying control gains, which are changing with control errors. They are designed to be

$$k_p = (\omega_c + \Delta\omega)^2, k_d = 2(\omega_c + \Delta\omega) \tag{10}$$

where $\Delta\omega$ is defined as

$$\Delta\omega = G|y_r - z_1| \tag{11}$$

where G is a positive gain.

By such design, controller bandwidths, which are changing with control errors, make the system response be more robust to disturbance.

Remark 1: LESO (5) is a particular case of the TESO (6), if $\rho_0 = \rho_\infty = 1$, $\dot{\rho}(t) \equiv 0$.

Remark 2: According to [27], let $\beta_1 = 3\omega_o, \beta_2 = 3\omega_o^2, \beta_3 = \omega_o^3$. Here, ω_o is the observer bandwidth. If a proper observer bandwidth ω_o is chosen, system performance can be greatly promoted.

Remark 3: With the help of a variable bandwidth controller, closed-loop tracking performance will be strengthened, especially in the steady phase when observer bandwidth is reduced so as to minimize the influence of sensor noises.

Closed-loop scheme of the VBADRC is given in Fig. 3. Next, the convergence of a TESO is discussed.

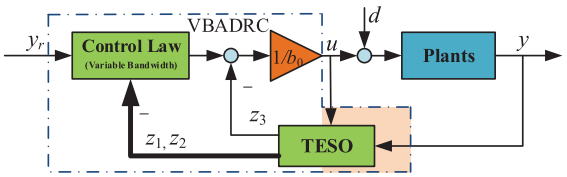

FIGURE 3. Structure of the 3rd order VBADRC.

2) CONVERGENCE OF A TESO

Let estimation errors of a TESO be

$$\begin{cases} e_1 = x_1 - z_1 \\ e_2 = x_2 - z_2 \\ e_3 = f - z_3 \end{cases} \tag{12}$$

According to system (3) and TESO (6), the estimation error dynamical system is

$$\dot{e}(t) = A_e(t)e(t) + B_2\dot{f}(\cdot) - \bar{B}_e(t)n(t) \tag{13}$$

where

$$B_e = \begin{bmatrix} 0 \\ \beta_2 \\ \beta_3 \end{bmatrix}, C_e = \begin{bmatrix} 1 \\ 0 \\ 0 \end{bmatrix},$$

$$B_2 = \begin{bmatrix} 0 \\ 0 \\ 1 \end{bmatrix}, \bar{B}_e(t) = \begin{bmatrix} \beta_1 \\ \beta_2\rho(t) \\ \beta_3\rho(t) \end{bmatrix},$$

$$\bar{A}_e = \begin{bmatrix} -\beta_1 & 1 & 0 \\ -\beta_2 & 0 & 1 \\ -\beta_3 & 0 & 0 \end{bmatrix}, e(t) = [e_1, e_2, e_3]^T,$$

$$A_e(t) = \begin{bmatrix} -\beta_1 & 1 & 0 \\ -\beta_2\rho(t) & 0 & 1 \\ -\beta_3\rho(t) & 0 & 0 \end{bmatrix} = \bar{A}_e - B_e C_e^T(\rho(t) - 1)$$

where $n(t)$ is the measurement noise. For an engineering system, it is reasonable to make following assumptions.

Assumption 1: $|\dot{f}(\cdot)| \le D_f$ [28], $|n(t)| \le D_n$, where D_f and D_n are positive constants.

Remark 4: It is impossible for displacements, velocity, mass, damping coefficient, and generation processes of hysteresis to change suddenly. Therefore, it is reasonable to assume change rate of the total disturbance is bounded.

Remark 5: For the measurement noise, it can be described in stochastic mathematics or deterministic mathematics. No matter what description approach is utilized, it is impossible for the noises to be unbounded in an engineering system. In addition, considering that the energy of a sensor is limited, the power of measurement noises is also limited in engineering. Therefore, like any other engineering system, it is reasonable to assume that the measurement noises introduced by sensors are bounded in a nanopositioning system.

Theorem 1: If Assumption 1 holds and let $0 < \rho_\infty \le \rho_0 < 3$, then estimation error $e(t)$ satisfies

$$\|e(t)\| \le \gamma_1 \exp(-\gamma_2 t)\|e(t_0)\| + \gamma_3(D_f + D_n)$$

where $\gamma_1, \gamma_2, \gamma_3$ are positive constants.

Proof: is given in Appendix A.

Theorem 1 depicts that estimation error of a TESO is bounded. From Theorem 1 and its proof, one can see that the upper bound of estimation errors consist of two parts. The first part depends on the initial error and the exponential decay rate. The Second one is related to tunable bandwidth of the observer (see the Proof in Appendix A for details), bound of the generalized disturbance and the measurement noise, respectively. Therefore, by choosing proper parameters, one can guarantee the convergence of a TESO. Moreover, it is worth pointing out that the limitation on the time-varying factor $\rho(t)$ is so mild that a practitioner only needs to keep $\rho(t) \in (0, 3)$.

3) TRANSIENT PERFORMANCE OF A TESO

Estimation and compensation of the generalized disturbance is crucial for the satisfied system performance. Numerous cases have confirmed that a LESO based LADRC ensure satisfactory transient performance. Thus, in initial state, the TESO should also guarantee the desired transient performance. This is confirmed as follows.

Let estimation errors of a LESO be $\bar{e}_1, \bar{e}_2, \bar{e}_3$, one has

$$\dot{\bar{e}}(t) = \bar{A}_e\bar{e} + B_2\dot{f}(\cdot) - \bar{B}_{le}n(t) \tag{14}$$

where $\bar{e} = [\bar{e}_1, \bar{e}_2, \bar{e}_3]^T, \bar{B}_{le} = [\beta_1, \beta_2, \beta_3]^T$.

Lemma 1 depicts the transient performance of a TESO.

Lemma 1 [25]: Let $\rho(t_0) = 1$ and $\bar{e}(0) = e(0)$, then estimation error of a TESO defined in (13) and estimation error of a LESO defined in (14) satisfies

$$\sup_{t\in[t_0,t^*]} \|e(t) - \bar{e}(t)\| \le \gamma_4(t^* - t_0) \sup_{t\in[t_0,t^*]} |\dot{\rho}(t)|$$

where t^* is an any given positive constant.

Lemma 1 confirms that difference between estimated errors of a TESO and those of a LESO is bounded.Additionally, the upper bound depends on the time span and the change rate of time-varying factor $\rho(t)$. When $\rho_0 = \rho_\infty = 1$, the change rate of $\rho(t)$ is zero, estimation errors of a TESO equal those of a LESO. By tuning $\dot{\rho}(t)$, $t \in [t_0, t^*]$, estimation errors of a TESO can be arbitrarily close to those of a LESO when $t \in [t_0, t^*]$. It signifies that, in the initial state, a TESO is similar to a LESO in estimating the generalized disturbance.

4) STEADY PERFORMANCE OF A TESO

Assume that estimation error of a TESO, $e(t)$, converges to $\underline{e}(t)$ as $t \to \infty$.

Let $\underline{e}(t) = [\underline{e}_1(t), \underline{e}_2(t), \underline{e}_3(t)]^T$, then

$$\begin{cases} \dot{\underline{e}}(t) = A_{e,\infty}\underline{e}(t) + B_2\dot{f}(\cdot) - \bar{B}_{e,\infty}n(t) \\ \underline{e}(0) = e(0) \end{cases}$$

where $A_{e,\infty} = \bar{A}_e - B_e C_e^T(\rho_\infty - 1)$, $\bar{B}_{e,\infty} = \lim_{t\to\infty} \bar{B}_e(t)$.

For a TESO, one has Lemma 2.

Lemma 2 [25]: By Assumption 1, $\lim_{t\to\infty} \|e(t) - \underline{e}(t)\| = 0$.

Lemma 2 shows that $e(t) \to \underline{e}(t)$, as $t \to \infty$. In other words, in steady state, estimation error of a TESO is $\underline{e}(t)$. On the other hand, estimation error of a LESO is $\bar{e}(t)$. Therefore, if one wants to see the difference of estimation error between a TESO and a LESO in steady state, one can just compare $\underline{e}(t)$ and $\bar{e}(t)$.

Thus, in steady state, by comparing $\underline{e}(t)$ with $\bar{e}(t)$, the advantage of a TESO on noise filtering can be clarified.

Define following Laplace transformations,

$$L[\bar{e}_1(t)] = \bar{E}_1(s), L[\bar{e}_2(t)] = \bar{E}_2(s), L[\bar{e}_3(t)] = \bar{E}_3(s)$$
$$L[\underline{e}_1(t)] = \underline{E}_1(s), L[\underline{e}_2(t)] = \underline{E}_2(s), L[\underline{e}_3(t)] = \underline{E}_3(s)$$

and $L[n(t)] = N(s)$.

Remark 6: It is reasonable to assume the measurement noise $n(t)$ is bounded. Based on such assumption, according to the existence of a Laplace transformation [29], for a bounded signal $n(t)$, its Laplace transformation $N(s)$ exists for the real part of complex variable s is positive, i.e. $Re(s) > 0$.

Then, the transfer functions between $\bar{E}(t)$, $\underline{E}(t)$ and $n(t)$ can be defined as

$$\begin{bmatrix} \frac{\bar{E}_1(s)}{N(s)} \\ \frac{\bar{E}_2(s)}{N(s)} \\ \frac{\bar{E}_3(s)}{N(s)} \end{bmatrix} = \frac{-1}{s^3 + \beta_1 s^2 + \beta_2 s + \beta_3} \begin{bmatrix} \beta_1 s^2 + \beta_2 s + \beta_3 \\ \beta_2 s^2 + \beta_3 s \\ \beta_3 s^2 \end{bmatrix} N(s)$$

and

$$\begin{bmatrix} \frac{\underline{E}_1(s)}{N(s)} \\ \frac{\underline{E}_2(s)}{N(s)} \\ \frac{\underline{E}_3(s)}{N(s)} \end{bmatrix} = \frac{-\rho_\infty}{s^3 + \beta_1 s^2 + \rho_\infty\beta_2 s + \rho_\infty\beta_3} \begin{bmatrix} \frac{1}{\rho_\infty}\beta_1 s^2 + \beta_2 s + \beta_3 \\ \beta_2 s^2 + \beta_3 s \\ \beta_3 s^2 \end{bmatrix} N(s)$$

Thus,

$$\lim_{s\to\infty} \frac{\underline{E}_2(s)}{N(s)} \Big/ \frac{\bar{E}_2(s)}{N(s)} = \rho_\infty < 1$$

and

$$\lim_{s\to\infty} \frac{\underline{E}_3(s)}{N(s)} \Big/ \frac{\bar{E}_3(s)}{N(s)} = \rho_\infty < 1$$

It quantitatively reveals that a TESO has better filtering performance than a LESO at high frequency range. In other words, the TESO can achieve better filtering performance in steady state.

From Lemma 1 and Lemma 2, one can see clearly that a TESO is able to obtain both similar estimation ability of the generalized disturbance in initial state and better noises filtering performance in steady state. Additionally, cooperated with a VBC, a VBADRC is constructed, and satisfied closed-loop tracking performance can also be guaranteed in the case of reducing the observer bandwidth.

Design procedures of the VBADRC are summarized in the subsequent section.

5) CLOSED-LOOP STABILITY BY THE VBADRC

Substituting control law (9) into system (3), one has

$$\begin{cases} \dot{x}_1 = x_2 \\ \dot{x}_2 = k_p(y_r - x_1) - k_d x_2 + k_p e_1 + k_d e_2 + e_3 \end{cases} \tag{15}$$

Define $r_1 = y_r$, $r_2 = \dot{y}_r$ and tracking errors $\varepsilon_i = r_i - x_i$, $i = 1, 2$. Then,

$$\begin{cases} \dot{\varepsilon}_1 = \dot{r}_1 - \dot{x}_1 = \varepsilon_2 \\ \dot{\varepsilon}_2 = \dot{r}_2 - \dot{x}_2 \\ \quad = \dot{r}_2 + k_d r_2 - k_p\varepsilon_1 - k_d\varepsilon_2 - k_p e_1 - k_d e_2 - e_3 \end{cases} \tag{16}$$

Define $\varepsilon = [\varepsilon_1, \varepsilon_2]^T$, and

$$A_\varepsilon = \begin{bmatrix} 0 & 1 \\ -k_p & -k_d \end{bmatrix}, B_r = \begin{bmatrix} 0 \\ 1 \end{bmatrix},$$
$$A_{\varepsilon+1} = \begin{bmatrix} 0 & 0 & 0 \\ -k_p & -k_d & -1 \end{bmatrix}$$

For $\Delta\omega \ge 0$, one has

$$\|A_\varepsilon\| \ge \left\|\underline{A}_\varepsilon\right\|, \|A_{\varepsilon+1}\| \ge \left\|\underline{A}_{\varepsilon+1}\right\|,$$
$$\underline{A}_\varepsilon = \begin{bmatrix} 0 & 1 \\ -k_{pl} & -k_{dl} \end{bmatrix}, \underline{A}_{\varepsilon+1} = \begin{bmatrix} 0 & 0 & 0 \\ -k_{pl} & -k_{dl} & -1 \end{bmatrix}.$$

Then, dynamics of tracking errors (16) can be rewritten as

$$\dot{\varepsilon}(t) = A_\varepsilon\varepsilon(t) + B_r r_0 + A_{\varepsilon+1}e(t) \tag{17}$$

where $r_0 = \dot{r}_2 + k_d r_2$. For a bounded set-value y_r, r_0 is also bounded.

Theorem 2: By the VBADRC, the closed-loop system is bounded input and bounded output (BIBO) stable, if proper parameters of the variable bandwidth controller and the time-varying extended state observer are chosen.

Proof Solving (17), one has

$$\varepsilon(t) = \exp(A_\varepsilon t)\varepsilon(0) + \int_0^t \exp(A_\varepsilon(t-\tau))(A_{\varepsilon+1}e(t) + B_r r_0)d\tau \quad (18)$$

When $0 < \bar{\lambda}_1 < \bar{\lambda}_2$ are the eigenvalues of A_ε and T is an invertible matrix, one has

$$\exp(A_\varepsilon t) = T diag\{\exp(-\bar{\lambda}_1 t), \exp(-\bar{\lambda}_2 t)\}T^{-1}$$
$$\|\exp(A_\varepsilon t)\| \le \|T\| \left\|T^{-1}\right\| \exp(-\bar{\lambda}_1 t) = \bar{\beta}\exp(-\bar{\lambda}_1 t)$$

and

$$\begin{aligned}
&||\varepsilon(t)|| = ||\exp(A_\varepsilon t)\varepsilon(0) + \\
&\int_0^t \exp(A_\varepsilon(t-\tau))(A_{\varepsilon+1}e(t) + B_r r_0)d\tau|| \\
&\le ||\exp(A_\varepsilon t)\varepsilon(0)|| + \\
&||\int_0^t \exp(A_\varepsilon(t-\tau))(A_{\varepsilon+1}e(t) + B_r r_0)d\tau|| \\
&\le \left\|\bar{\beta}\exp(-\bar{\lambda}_1 t)\right\| \|\varepsilon(0)\| + \\
&(\|A_{\varepsilon+1}\| \|e_0\| + \|B_r\| \|r_0\|) \left\|\bar{\beta}\right\| \left\|\int_0^t \exp(-\bar{\lambda}_1(t-\tau))d\tau\right\| \\
&\le \left\|\bar{\beta}\right\| \|\varepsilon(0)\| + \\
&(\|A_{\varepsilon+1}\| \|e_0\| + r_0) \left\|\bar{\beta}\right\| \left\|\frac{1}{\bar{\lambda}_1}[1 - \exp(-\bar{\lambda}_1 t)]\right\| \\
&\le \left\|\bar{\beta}\right\| \|\varepsilon(0)\| + (\|A_{\varepsilon+1}\| \|e_0\| + r_0) \left\|\bar{\beta}\right\| \left\|\frac{1}{\bar{\lambda}_1}\right\| = \varepsilon_0
\end{aligned}$$

It shows that the control errors of a VBADRC are bounded, if estimation errors of a TESO are bounded. Moreover, the tracking errors are associated with initial tracking error $\varepsilon(0)$, controller parameters k_p, k_d and estimation error e_0 of the TESO.

6) DESIGN PROCEDURES OF THE VBADRC

For the VBADRC, $b_0, k_p, k_d, G, \beta_1, \beta_2, \beta_3, \rho_0, \rho_\infty, l$ are tunable parameters. Design procedures can be summarized as,

Step 1. Controller and observer can be designed according to (9), (10), (11), and (6);

Step 2. Let $k_p = (\omega_c + \Delta\omega)^2$, $k_d = 2(\omega_c + \Delta\omega)$, $\beta_1 = 3\omega_o$, $\beta_2 = 3\omega_o^2$, $\beta_3 = \omega_o^3$, here, ω_c is the controller bandwidth, and ω_o is the observer bandwidth;

Step 3. Determine $\Delta\omega$ and G according to (11);

Step 4. Determine ρ_0, ρ_∞, l and b_0;

Step 5. Adjust $b_0, \omega_c, G, \omega_o, \rho_0, \rho_\infty, l$ so as to satisfy the requirements.

Based on the analysis and design procedures, numerical and experimental results are presented in following Sections.

IV. SIMULATION RESULTS

In this section, the VBADRC is verified by numerical simulations. Here, a Bouc-Wen hysteresis model [30] is utilized to simulate physical properties of the hysteresis. After the identification, one has the Bouc-Wen model,

$$\begin{cases} x_h = 0.91u + 0.45h \\ \dot{h} = -0.87\dot{u} + 0.14|\dot{u}||h|^2 h + 0.13\dot{u}|h|^3 \end{cases} \quad (19)$$

The first equation of (19) depicts the relationship among a driving signal u, a hysteretic variable h and the hysteresis output signal x_h. The second state equation shows that the hysteretic variable h varies depending on the input u and its changing rate $\dot{u}$. A hysteresis curve is given in Fig. 4, and the root mean square error (RMSE) is 0.6740.

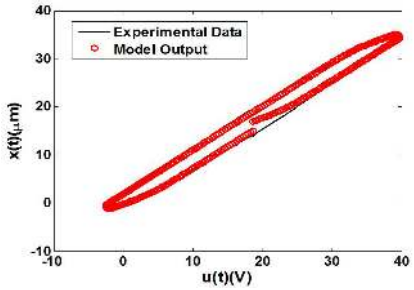

FIGURE 4. Hysteresis loops between the experimental data and the model output.

Similarly, after the identification, linear dynamics of the stage is

$$G(s) = \frac{9.207 \times 10^5}{s^2 + 332.4s + 1.296 \times 10^6} \quad (20)$$

According to the cascade structure of a piezo-actuated nanopositioning stage shown in Fig. 1 [26], hysteresis model depicted by (19) and linear model depicted by (20) are connected in series to simulate the dynamics of a positioning stage in simulations. The LADRC and the VBADRC are designed respectively. Numerical studies has been performed to evaluate the motion tracking performance.

To quantify the tracking performance, mean absolute error (MAE), root mean square error (RMSE), and integral of time multiplied absolute value of error (ITAE) are defined as

$$\begin{cases} MAE = \frac{1}{k}\sum_{i=1}^{k} e_{track\_i} \\ RMSE = \sqrt{\frac{1}{k}\sum_{i=1}^{k} e_{track\_i}^2} \\ ITAE = \sum_{i=1}^{k} \left|e_{track\_i}\right| t_i T \end{cases} \quad (21)$$

where k is the number of the tracking error $e_{track} = y_r - y$, t_i is the very time corresponding to the tracking error e_{track_i}, T is the sample period. In simulations, the sample time interval is selected to be $T = 0.0001\ s$.

Step signal and sine signal listed in Table 1 are taken as the desired trajectories (set-values). Control parameters are given in Table 2. Performance indexes defined in (21) are presented

TABLE 1. Set-values taken in simulations and experiments.

Set-values	Value (μm)
Step signal	$y_r = \begin{cases} 4 & t \geq 0 \\ 0 & t < 0 \end{cases}$
Sine signal	$y_r = 2\sin(2\pi t) + 3$

TABLE 2. Control parameters of the LADRC and the VBADRC (Simulation cases).

Controllers	b_0	ω_o	ω_c	ρ_0	ρ_∞	l	G
LADRC	6×10^6	8×10^3	600	-	-	-	-
VBADRC	6×10^6	8×10^3	600	1	0.5	5	350

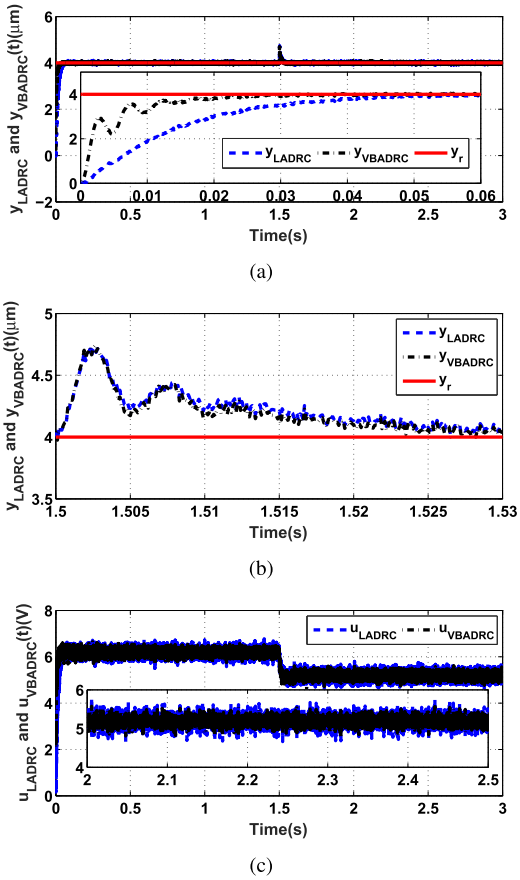

FIGURE 5. Step responses (for simulations). (a) Tracking performance. (b) Disturbance rejection. (c) Control efforts.

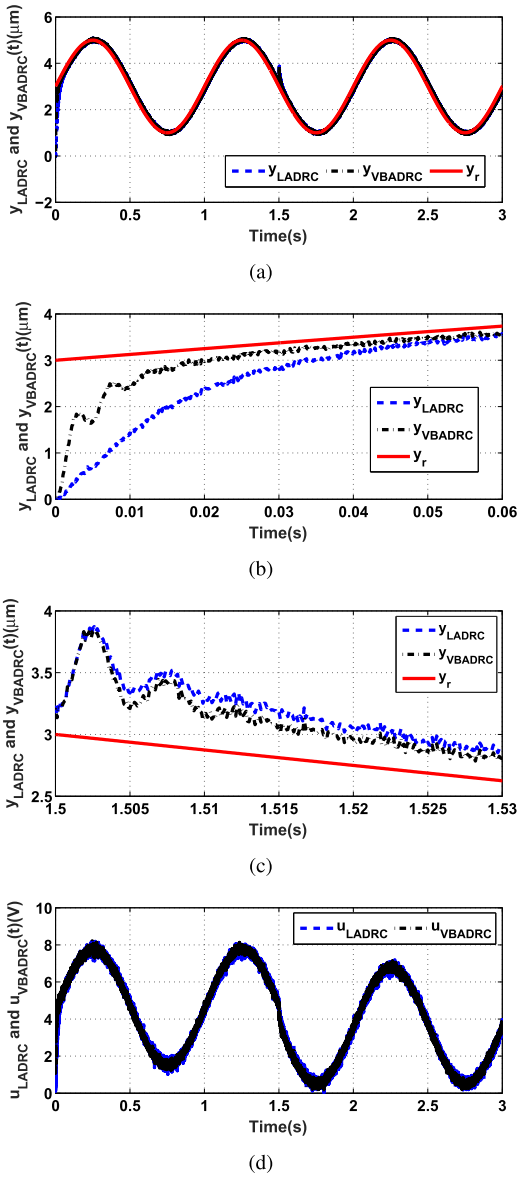

FIGURE 6. Sinusoidal responses (for simulations). (a) Tracking performance. (b) Rising performance. (c) Disturbance rejection. (d) Control efforts.

in Table 3. A random number with variance of 6×10^{-4} is taken to simulate the sensor noises. A constant disturbance with amplitude of 1 is introduced at $t = 1.5s$. Simulation results are shown in Figs. 5 and 6.

Figs. 5 (a) and 6 (b) show that responses of the VBADRC are much faster than the one of the LADRC. Figs. 5 (b) and 6 (c) present that the VBADRC is able to recover faster in presence of disturbance, even if the bandwidth of a TESO is reduced. From Figs. 5 (c) and 6 (d), one can see that, by a TESO, control signals of the VBADRC is less influenced by sensor noises. Numerical results show that the VBC is able to strengthen the tracking and disturbance rejection ability, when a TESO reduces its bandwidth so as to minimized the effect of sensor noises. Via the cooperation of a VBC and a TESO, the VBADRC is able to guarantee desired performance. Tracking performance quantified by MAE, RMSE and ITAE is also utilized to compare the difference between the VBADRC and the LADRC. Much smaller MAE, RMSE and ITAE values listed in Table 3 confirm the advantages of the VBADRC.

In Section V, experimental results are also presented to verify the VBADRC.

V. EXPERIMENTAL RESULTS

A. EXPERIMENTAL SETUP

In this section, a series of experimental studies have been performed on a piezoelectric-driven nanopositioning system.

TABLE 3. Performance indexes of tracking errors: comparisons of tracking performance (Simulation cases).

Set-values	Performance	LADRC	VBADRC	Improvements
Step signal	MAE	0.0421	0.0281	33.43%
	RMSE	0.2094	0.1086	48.14%
	ITAE	0.1051	0.0988	5.99%
Sine signal	MAE	0.1334	0.1126	15.63%
	RMSE	0.2131	0.1511	29.08%
	ITAE	0.5364	0.4867	9.26%

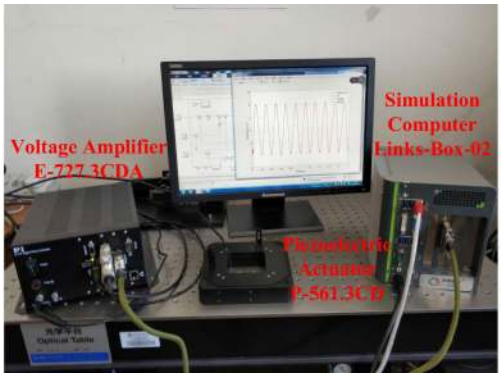

FIGURE 7. Experimental setup of a piezoelectric nanopositioning system.

TABLE 4. Set-values and control parameters (Experiment cases).

Set-values	Controllers	b_0	ω_o	ω_c	ρ_0	ρ_∞	l	G
Step signal	LADRC	1×10^6	400	100	-	-	-	-
	VBADRC	1×10^6	400	100	1	0.5	5	70
Sine signal	LADRC	1×10^6	1500	300	-	-	-	-
	VBADRC	1×10^6	1500	300	1	0.5	5	300

TABLE 5. Performance indexes of tracking errors: comparisons of tracking performance (Experiment cases).

Set-values	Performance	LADRC	VBADRC	Improvements
Step signal	MAE	0.2158	0.0913	57.68%
	RMSE	0.6179	0.3448	44.21%
	ITAE	0.2933	0.2292	21.85%
Sine signal	MAE	0.0769	0.0750	2.42%
	RMSE	0.0902	0.0876	2.84%
	ITAE	0.3598	0.3513	2.37%

The experimental setup taken in this work is given in Fig. 7. Experiments have been performed on a commercial PZT driven stage (P-561.3CD, Physik Instrumente, Karlsruhe, Germany). It is connected to a voltage amplifier. The stage can perform horizontal movements up to $100\mu m$. Output displacements are measured by a built-in capacitive displacement sensor (resolution: $0.8\mu m$). A LINKS-RT hardware-in-the-loop system controlled by a host computer produces voltages to drive the stage. The sampling interval in experiments is set to be 0.0001 s.

B. RESULTS

In this section, signals listed in Table 1 are also taken as the desired trajectories (set-values). Control parameters are given in Table 4. Experimental results are presented in Fig. 8 and Fig. 9. Performance indexes are shown in Table 5.

From Fig. 8, one can see that, with the same b_0, ω_c, and ω_o, the VBADRC has a much faster response than the LADRC.

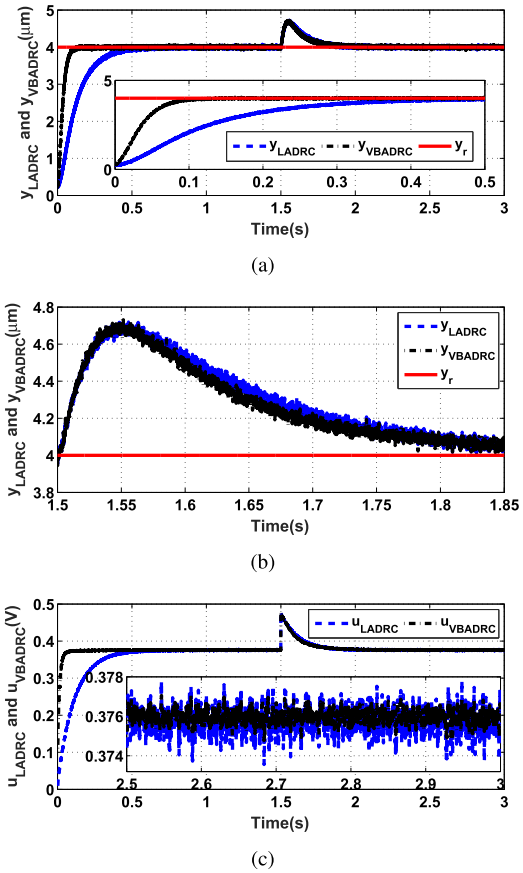

FIGURE 8. Step responses (for experiments). (a) Tracking performance. (b) Disturbance rejection. (c) Control efforts.

Rising time of the VBADRC is less than 0.1 seconds, on the other hand, rising time of the LADRC is almost three times than the one of the VBADRC. Figs. 8 (b) and Fig. 9 (b) present the disturbance rejection ability. Although observer bandwidth of the TESO is reduced half in the steady state, the disturbance rejection ability is not weakened as a result of the variable bandwidth controller designed in the VBADRC. Fig. 8 (c) and Fig. 9 (c) illustrate that, by comparison with the LADRC, less fluctuations exist in control signals of the VBADRC. MAE, RMSE, and IAE values defined in (21) are listed in Table 5. From the data presented in Table 5, it is obvious that, by the VBADRC, smaller MAE, RMSE, and IAE values can be obtained for both step and sine references. It means that better precision can be achieved by the VBADRC. Moreover, Fig. 9 (d) shows that not only the chattering range but also the peaks of control signals are reduced by the VBADRC.

C. DISCUSSIONS

Accuracy is a key issue in precision and ultrahigh-precision manufacturing. PZT introduces inherent hysteresis, creep and lightly damped resonant dynamics, which greatly decrease the accuracy of positioning. At the same time, the sensor noise is also a critical factor in determining the accuracy. Therefore,

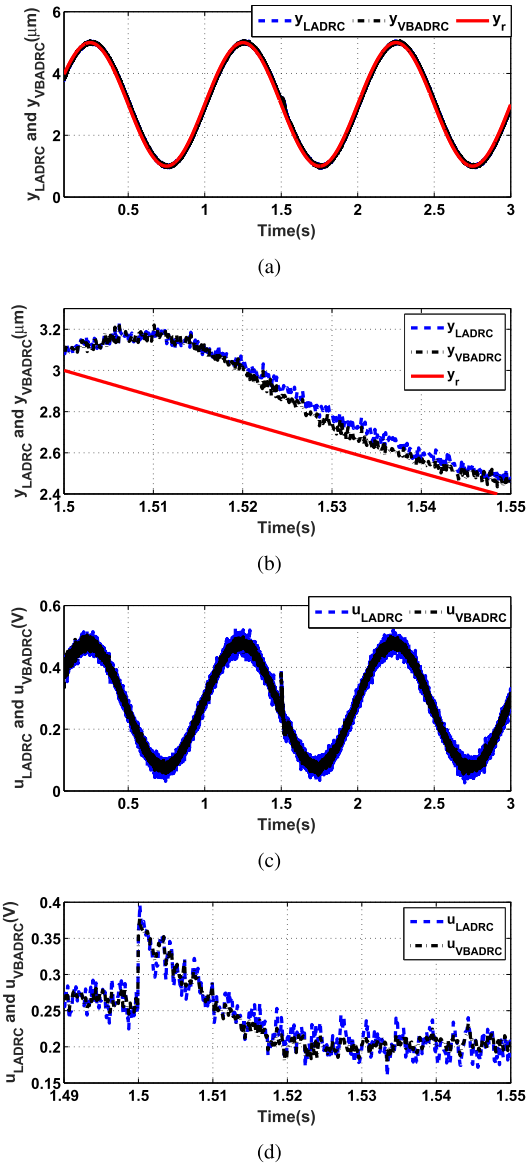

FIGURE 9. Sinusoidal responses (for experiments). (a) Tracking performance. (b) Disturbance rejection. (c) Control efforts. (d) Magnified of (c).

it is significant that addressing both nonlinearities of a PZT and the sensor noises.

From Figs. 8-9, and Table 5, a distinct view can be drawn. The VBADRC can track reference signals as accurate as the LADRC does. Exactly, it is more accurate than the LADRC. Simultaneously, it is also more effective in reducing the impact of noises. Figs. 5(c), 6(d), 8(c), 9(c), and 9(d) depict a vivid picture that, as a result of the TESO, influence of the noises on control signals is reduced effectively. Table 6 lists the root mean square error of control signals in steady state.

RMSU is short for the root mean square error of the control signal u, and it is calculated as

$$RMSU = \sqrt{\frac{1}{N - N_0} \sum_{i=N_0}^{N} (u_i - \bar{u}_i)^2}$$

TABLE 6. RMSUs of LADRC and VBADRC.

	Set-values	LADRC	VBADRC	Improvements
Simulation	Step signal	0.1572	0.1130	28.09%
	Sine signal	0.1572	0.1144	27.21%
Experiment	Step signal	5.953×10^{-4}	3.115×10^{-4}	47.67%
	Sine signal	0.0144	0.0080	44.73%

where, $N = 30000, N_0 = 20000$, u_i is the control signal of the ith time, and $\bar{u}_i$ is the mean of a hundred continuous control signals.

Both figures and data given in Table 6 confirm that the impact of noises is greatly decreased. Moreover, it is worth pointing out that no filter or other special structures are necessary to deal with noises. Therefore, there is no additional phase delays. A time-varying factor $\rho(t)$ guarantees desired performance.

In simulations and experiments, parameters of the VBADRC and the LADRC are similar. Specially, ρ_0, ρ_∞ and l are taken the same values. Data listed in Table 3 differs from the ones listed in Table 5. It means that the model of a nanopositioning stage and the stage itself are different. Fortunately, both the VBADRC and the LADRC are powerful in dealing with uncertainties and unmodelled dynamics of the stage.

Nevertheless, it is admitted that the TESO is sensitive to external disturbances, since its bandwidth is narrowed down. Therefore, ρ_0, ρ_∞ and l are critical to the performance of a TESO. If PD controller is still utilized, then there should be some trade-off between the disturbance rejection and the noise tolerance. However, in this paper, a variable bandwidth controller is designed. Controller bandwidth is increased to guarantee the tracking performance when the observer bandwidth is narrowed down to minimize the influence of sensor noises. Therefore, by combination of the VBC and the TESO, both tracking accuracy and noise suppression can be addressed to some extent.

VI. CONCLUSION

Hysteresis, external disturbances and measurement noises are challenges in improving the positioning accuracy of a piezoelectric actuator driven nanoposotioning stage. In this paper, an active disturbance rejection control is designed to address those challenges. In order to minimize the influence of measurement noises, a time-varying extended state observer is proposed. Simultaneously, for the sake of guaranteeing the tracking performance in presence of reducing the observer bandwidth, a variable bandwidth controller is proposed to keep the tracking accuracy by changing the controller bandwidth with the control errors. Theoretical results on the TESO and the VBADRC guarantees convergence of the TESO and closed-loop stability of the VBADRC. Numerical and experimental results show advantages of the VBADRC over the LADRC. From the results, one can see that the VBADRC is a practical solution to deal with both disturbances and measurement noises existing in a nanopositioning stage.

APPENDIX I. PROOF OF THEOREM 1

Proof Firstly, it will be shown that there exists a positive constant matrix P_e and a positive constant c_0 such that

$$A_e^T(t)P_e + P_eA_e(t) \leq -c_0P_e$$

Define $Q_1(s) = C_e^T(sI - \bar{A}_e)^{-1}B_e$, it can be verified that

$$Q_1(j\omega) = \frac{{\omega_o}^3}{(j\omega + \omega_o)^3} = \frac{1}{(j\frac{\omega}{\omega_o} + 1)^3} = \frac{1}{\left(\left\|\frac{\omega}{\omega_o}\right\|^2 + 1\right)^{3/2}} e^{-j\theta}$$

and $\theta = \arctan(\frac{\omega}{\omega_0})$, $\theta \in (0, \frac{\pi}{2})$.

Note that the Nyquist plot of $\frac{1}{(j\frac{\omega}{\omega_o} + 1)^3}$ lies in the closed disk $D_n(-0.5, 1)$, whose diameter is the line segment connecting points $-0.5 + j0$ and $1 + j0$. Thus, the circle criterion means that $Q_2(s) \triangleq \frac{1 + \alpha_4 Q_1(s)}{1 + \alpha_3 Q_1(s)}$ is strictly positive real when $[\alpha_3, \alpha_4] \subset (-1, 2)$.

Since $Q_2(s)$ has following state-space realization

$$\begin{cases} \dot{\zeta} = (\bar{A}_e - \alpha_4 B_e C_e^T)\zeta + B_e\bar{u}^* \\ \bar{y}^* = (\alpha_3 - \alpha_4)C_e^T\zeta + \bar{u}^* \end{cases}$$

There exists a positive matrix P_e and a vector L such that

$$\begin{cases} (\bar{A}_e - \alpha_4 B_e C_e^T)^T P_e + P_e(\bar{A}_e - \alpha_4 B_e C_e^T) \\ \qquad\qquad = -LL^T - c_0P_e \\ P_eB_e = (\alpha_3 - \alpha_4)C_e - \sqrt{2}L \end{cases}$$

Note that $-1 < \lim_{t\to\infty} \rho(t) - 1 \leq \rho(t) - 1 \leq \rho_0 - 1 < 2$, then

$$\begin{aligned} &{A_e}^T P_e + P_eA_e \\ &= (\bar{A}_e - B_eC_e^T(\rho(t) - 1))^T P_e + P_e(\bar{A}_e - B_eC_e^T(\rho(t) - 1)) \\ &\leq -LL^T - c_0P_e - C_eB_e^TP_e(\rho(t) - 1 - \alpha_4) \\ &\quad -P_eB_eC_e^T(\rho(t) - 1 - \alpha_4) \\ &\leq -c_0P_e - LL^T - C_e[(\alpha_3 - \alpha_4)C_e - \sqrt{2}L]^T(\rho(t) - 1 - \alpha_4) \\ &\quad -[(\alpha_3 - \alpha_4)C_e - \sqrt{2}L]C_e^T(\rho(t) - 1 - \alpha_4) \\ &= -c_0P_e - (\sqrt{2}(\alpha_4 - (\rho(t) - 1))C_e - L)^T(\sqrt{2}(\alpha_4 \\ &\quad -(\rho(t) - 1))C_e - L) \leq -c_0P_e \end{aligned}$$

Let $V(e) = e^TP_ee$, then

$$\begin{aligned} &\frac{dV(e)}{dt} \\ &= e^T(P_eA_e + {A_e}^TP_e)e - 2e^TP_eB_e\rho(t)n + 2e^TP_eB_2\dot{f}(\cdot) \\ &\leq c_0V(e) + 2\|e\|\|P_e\|(\|B_e\| + \|B_2\|)(D_f + D_n) \end{aligned}$$

which leads to

$$\frac{d\sqrt{V(e)}}{dt} \leq -\frac{c_0}{2}\sqrt{V(e)} + \frac{\|e\|}{\sqrt{V(e)}}\|P_e\|(\|B_e\| + \|B_2\|)(D_f + D_n)$$

Let the maximal eigenvalue and minimal eigenvalue of P_e be c_1 and c_2, respectively. One has

$$\frac{d\sqrt{V(e)}}{dt} \leq -\frac{c_0}{2}\sqrt{V(e)} + \sqrt{\frac{c_2}{c_1}}(\|B_e\| + \|B_2\|)(D_f + D_n)$$

Then, the comparison principle shows

$$\begin{aligned} \sqrt{V(e)} \leq \exp(-\frac{c_0}{2}t)\sqrt{V(e(t_0))} + \frac{2\sqrt{c_2}}{c_0\sqrt{c_1}}(\|B_e\| + \|B_2\|) \\ \times(D_f + D_n) \end{aligned}$$

Consequently,

$$\begin{aligned} \|e(t)\| \leq \frac{\sqrt{c_2}}{\sqrt{c_1}}\exp(-\frac{c_0}{2}t)\|e(t_0)\| + \frac{2\sqrt{c_2}}{c_0\sqrt{c_1}}(\|B_e\| + \|B_2\|) \\ \times(D_f + D_n) \end{aligned}$$

Let $\gamma_1 = \frac{\sqrt{c_2}}{\sqrt{c_1}}$, $\gamma_2 = \frac{c_0}{2}$, $\gamma_3 = \frac{2\sqrt{c_2}}{c_0\sqrt{c_1}}(\|B_e\| + \|B_2\|)$, one has

$$\|e(t)\| \leq \gamma_1\exp(-\gamma_2 t)\|e(t_0)\| + \gamma_3(D_f + D_n).$$

REFERENCES

[1] Z. Wang, A. Witthauer, Q. Zou, G.-Y. Kim, and L. Faidley, "Control of a Magnetostrictive-Actuator-Based micromachining system for optimal high-speed microforming process," *IEEE/ASME Trans. Mechatronics*, vol. 20, no. 3, pp. 1046–1055, Jun. 2015.
[2] G. Yan, Y. Liu, and Z. H. Feng, "A dual-stage piezoelectric stack for high-speed and long-range actuation," *IEEE/ASME Trans. Mechatronics*, vol. 20, no. 5, pp. 2637–2641, Oct. 2015.
[3] J. Mynderse and G. T.-C. Chiu, "Two-degree-of-freedom hysteresis compensation for a dynamic mirror actuator," *IEEE/ASME Trans. Mechatronics*, vol. 21, no. 1, pp. 29–37, Feb. 2016.
[4] G.-Y. Gu, L.-M. Zhu, C.-Y. Su, H. Ding, and S. Fatikow, "Modeling and control of piezo-actuated nanopositioning stages: A survey," *IEEE Trans. Autom. Sci. Eng.*, vol. 13, no. 1, pp. 313–332, Jan. 2016.
[5] V. Hassani, T. Tjahjowidodo, and T. N. Do, "A survey on hysteresis modeling, identification and control," *Mech. Syst. Signal Process.*, vol. 49, nos. 1–2, pp. 209–233, Dec. 2014.
[6] Y. Cao and X. B. Chen, "A survey of modeling and control issues for piezo-electric actuators," *J. Dyn. Syst., Meas., Control*, vol. 137, no. 1, pp. 01400101–01400113, Jan. 2015.
[7] M. S. Rana, H. R. Pota, and I. R. Petersen, "A survey of methods used to control piezoelectric tube scanners in high-speed AFM imaging," *Asian J. Control*, vol. 20, no. 4, pp. 1379–1399, Jul. 2018.
[8] W. S. Nagel, G. M. Clayton, and K. K. Leang, "Master-slave control with hysteresis inversion for dual-stage nanopositioning systems," in *Proc. Amer. Control Conf. (ACC)*, Jul. 2016, pp. 655–660.
[9] G. Gu, L.-M. Zhu, and C.-Y. Su, "Modeling and compensation of asymmetric hysteresis nonlinearity for piezoceramic actuators with a modified Prandtl–Ishlinskii model," *IEEE Trans. Ind. Electron.*, vol. 61, no. 3, pp. 1583–1595, Mar. 2014.
[10] L. Li, C.-X. Li, G. Gu, and L.-M. Zhu, "Positive acceleration, velocity and position feedback based damping control approach for piezo-actuated nanopositioning stages," *Mechatronics*, vol. 47, pp. 97–104, Nov. 2017.
[11] L. Cheng, W. Liu, Z.-G. Hou, T. Huang, J. Yu, and M. Tan, "An adaptive Takagi–Sugeno fuzzy model-based predictive controller for piezoelectric actuators," *IEEE Trans. Ind. Electron.*, vol. 64, no. 4, pp. 3048–3058, Apr. 2017.
[12] Q. Xu, "Continuous integral terminal third-order sliding mode motion control for piezoelectric nanopositioning system," *IEEE/ASME Trans. Mechatronics*, vol. 22, no. 4, pp. 1828–1838, Aug. 2017.

[13] C.-X. Li, Y. Ding, G.-Y. Gu, and L.-M. Zhu, "Damping control of piezo-actuated nanopositioning stages with recursive delayed position feedback," *IEEE/ASME Trans. Mechatronics*, vol. 22, no. 2, pp. 855–864, Apr. 2017.
[14] J. Y. Peng and X. B. Chen, "Integrated PID-based sliding mode state estimation and control for piezoelectric actuators," *IEEE/ASME Trans. Mechatronics*, vol. 19, no. 1, pp. 88–99, Feb. 2014.
[15] J. P. Mishra, Q. Xu, X. Yu, and M. Jalili, "Precision position tracking for piezoelectric-driven motion system using continuous third-order sliding mode control," *IEEE/ASME Trans. Mechatronics*, vol. 23, no. 4, pp. 1521–1531, Aug. 2018.
[16] H. Ghafarirad, S. M. Rezaei, A. Abdullah, M. Zareinejad, and M. Saadat, "Observer-based sliding mode control with adaptive perturbation estimation for micropositioning actuators," *Precis. Eng.*, vol. 35, no. 2, pp. 271–281, Apr. 2011.
[17] H. Tang and Y. Li, "Development and active disturbance rejection control of a compliant micro-/Nanopositioning piezostage with dual mode," *IEEE Trans. Ind. Electron.*, vol. 61, no. 3, pp. 1475–1492, Mar. 2014.
[18] Y. Yuan, Y. Yu, Z. Wang, and L. Guo, "A sampled-data approach to nonlinear eso-based active disturbance rejection control for pneumatic muscle actuator systems with actuator saturations," *IEEE Trans. Ind. Electron.*, vol. 66, no. 6, pp. 4608–4617, Jun. 2019.
[19] H. Coral-Enriquez, J. Cortés-Romero, and S. A. Dorado-Rojas, "Rejection of varying-frequency periodic load disturbances in wind-turbines through active disturbance rejection-based control," *Renew. Energy*, vol. 141, pp. 217–235, Oct. 2019.
[20] Z. Chu, C. Wu, and N. Sepehri, "Active disturbance rejection control applied to high-order systems with parametric uncertainties," *Int. J. Control, Autom. Syst.*, vol. 17, no. 6, pp. 1483–1493, Jun. 2019.
[21] J. Arcos-Legarda, J. Cortes-Romero, A. Beltran-Pulido, and A. Tovar, "Hybrid disturbance rejection control of dynamic bipedal robots," *Multibody Syst. Dyn.*, vol. 46, no. 3, pp. 281–306, Jul. 2019.
[22] Z. Pu, R. Yuan, J. Yi, and X. Tan, "A class of adaptive extended state observers for nonlinear disturbed systems," *IEEE Trans. Ind. Electron.*, vol. 62, no. 9, pp. 5858–5869, Sep. 2015.
[23] Z.-L. Zhao and B.-Z. Guo, "On active disturbance rejection control for nonlinear systems using time-varying gain," *Eur. J. Control*, vol. 23, pp. 62–70, May 2015.
[24] W. Xue, W. Bai, S. Yang, K. Song, Y. Huang, and H. Xie, "ADRC with adaptive extended state observer and its application to Air–Fuel ratio control in gasoline engines," *IEEE Trans. Ind. Electron.*, vol. 62, no. 9, pp. 5847–5857, Sep. 2015.
[25] W. Wei, W. Xue, and D. Li, "On disturbance rejection in magnetic levitation," *Control Eng. Pract.*, vol. 82, pp. 24–35, Jan. 2019.
[26] G.-Y. Gu, L.-M. Zhu, C.-Y. Su, and H. Ding, "Motion control of piezoelectric positioning stages: Modeling, controller design, and experimental evaluation," *IEEE/ASME Trans. Mechatronics*, vol. 18, no. 5, pp. 1459–1471, Oct. 2013.
[27] Z. Gao, "Scaling and bandwidth-parameterization based controller tuning," in *Proc. Amer. Control Conf.*, 2003, pp. 1–8.
[28] H. J. M. T. S. Adriaens, W. L. De Koning, and R. Banning, "Modeling piezoelectric actuators," *IEEE/ASME Trans. Mechatronics*, vol. 5, no. 4, pp. 331–341, Dec. 2000.
[29] C. Richard Dorf and H. Robert Bishop, "Mathematical models of systems," in *Modern Control System*, 12th ed. Upper Saddle River, NJ, USA: Prentice-Hall, 2011, ch. 2, sec. 2.4, pp. 58–59.
[30] F. Ikhouane, V. Mañosa, and J. Rodellar, "Dynamic properties of the hysteretic Bouc-Wen model," *Syst. Control Lett.*, vol. 56, no. 3, pp. 197–205, Mar. 2007.

WEI WEI received the B.S. degree in automation from the School of Information Engineering, Nanchang University, Nanchang, China, in 2005, and the Ph.D. degree in control theory and control engineering from the University of Science and Technology Beijing (USTB), Beijing, China, in 2010.

From September 2013 to December 2013, he was a Visiting Scholar with the University College Cork (UCC), Ireland. From September 2015 to June 2016, he was a Visiting Scholar with Beihang University, China. Since 2010, he has been with the School of Computer and Information Engineering, Beijing Technology and Business University (BTBU), Beijing, China. He is currently a Professor with BTBU. He is the author of three books and more than 50 refereed journal and conference papers. He holds three patents. His current research interests include active disturbance rejection control, learning control, and their applications.

Dr. Wei received the Wentsun Wu Artificial Intelligence Science and Technology Progress Award, in 2017.

PENGFEI XIA received the B.S. degree in automation from the Anhui University of Science and Technology, in 2017. He is currently pursuing the master's degree in control theory and control engineering with the Beijing Technology and Business University (BTBU). His major research directions are active disturbance rejection control and its applications.

WENCHAO XUE (Member, IEEE) received the B.S. degree in applied mathematics from Nankai University, in 2007, and the Ph.D. degree in control theory from the Academy of Mathematics and Systems Science (AMSS), Chinese Academy of Sciences (CAS), in 2012. He is currently an Associate Professor of Academy of AMSS, CAS. His research interests include active disturbance rejection control, nonlinear uncertain systems control, and nonlinear uncertain systems filtering.

MIN ZUO received the Ph.D. degree in computer applications technology from the University of Science and Technology Beijing, in 2011.

Since 1997, he has been with the School of Computer and Information Engineering, Beijing Technology and Business University (BTBU), Beijing, China. He is currently a Professor with BTBU. As a first author, he has published more than ten articles indexed by SCI or EI, in recent three years. His current research interests include intelligent control, intelligent information management, and artificial intelligence.